Quaternary Geochronology 73 (2022) 101402

Contents lists available at ScienceDirect

Quaternary Geochronology

journal homepage: www.elsevier.com/locate/quageo

Luminescence dating of Enigmatic rock structures in New England, USA

James K. Feathers [a,*], Marine Frouin [b], Tristan G. Bench [c]

[a] Luminescence Dating Laboratory, Department of Anthropology, University of Washington, Box 353412, Seattle, WA, 98195-3412, USA
[b] Department of Geosciences, Stony Brook University, Stony Brook, NY, 11794-2100, USA
[c] Department of Earth and Space Sciences, University of Washington, Seattle, WA, 98195, USA

ARTICLE INFO

Keywords:
Luminescence dating
Quartz vs feldspars
Rock structures
New England

ABSTRACT

Enigmatic rock structures in the form of walls, chambers, tunnels, and cairns are common archaeological features in northeastern United States, but the age of their construction is mostly unknown. Debate persists as to whether they are colonial or pre-colonial in age. Luminescence dating was applied at several sites to sediments underneath the rocks or to the rocks themselves. Sediment ages obtained from potassium feldspars using IRSL place their construction in the late 16th century, just before sustained colonial settlement. Sediment ages obtained from quartz using OSL place their construction later, but the much weaker quartz signals have issues, primarily the prevalence of a slower bleaching component. These raise questions on the credibility of the quartz ages. The age from one rock, also using IRSL, supports the K-feldspar sediment ages. The evidence suggests a pre-colonial construction, by ancestors of modern native Americans.

1. Introduction

Enigmatic rock structures, in the form of walls, cairns, tunnels and chambers, made by piling up locally available rocks, are common archaeological features in the northeastern United States. One list mentions 5550 such sites (Hoffman, 2019). Professional archaeologists have traditionally attributed these structures to European colonial activity (Feder 2019; Ives, 2013, 2015; Neudorfer 1979), but others, principally interested amateurs and some native Americans, assume prehistoric origins (e.g., Moore and Weiss, 2016). Chronological evidence is scarce: associated artifacts are rare and most radiocarbon dates also have uncertain associations. Luminescence dating, applied to sediments associated with stone structures in Massachusetts and Rhode Island obtained dates in the prehistoric range of AD 1450–1650 (Mahan et al., 2015, Mahan, 2020). Here we report results of a systematic luminescence study dating sediments and stones across New England.

2. Samples

In 2020-1 samples were collected for luminescence dating from more than twenty rock structure sites in seven states. This report presents results of 12 sediment samples and seven rock samples from eleven sites in Rhode Island, Connecticut, New Hampshire, and New York (Table 1). A map and photos of the sampling locations are given in the supplemental data (Figs. S1 and S2).

Eleven sediment samples were collected directly underneath a rock forming part of the structure. These sediments in most cases formed the ground surface prior to building the structure. At that time, bioturbation and pedoturbation continually brought grains to the surface where they were exposed to sunlight (Feathers et al., 2015). A major turbation agent in this forested environment is likely tree fall, but other agents including burrowing animals and freeze-thaw processes were no doubt also involved. With rock placement, it is assumed grains were no longer brought to the surface, staying buried, thus providing a way to date this placement. This assumption will be explored further on. The sediments may not have formed the original ground surface for some samples if the builders had first dug out a trench in which the rocks were placed. This is most evident at Hunt's Brook Souterrain, where the sediments under the rocks are 2 m below the current surface. In this case, anthropogenic digging would have zeroed some of the grains. One sediment sample (UW4098) was collected on top of the main chamber at America's Stonehenge, which provides only a minimum age for the chamber construction.

Because only some grains were fully exposed before rock placement, only the youngest grains will provide an accurate date. This requires determining equivalent dose on single grains of sand.

At first, sediment samples were collected by driving a 2.5 cm-diameter steel pipe horizontally under the rock to control the depth of

* Corresponding author.
E-mail address: jimf@uw.edu (J.K. Feathers).

https://doi.org/10.1016/j.quageo.2022.101402
Received 28 December 2021; Received in revised form 27 June 2022; Accepted 2 September 2022
Available online 7 September 2022

Table 1
Details on the sediment and rock samples dated in this study.

UW lab #	Site	State	Structure type	Sample type	Sampling method
UW4076	Madison Lithic	CT	wall	sediment	pipe
UW4077	Madison Lithic	CT	small platform	sediment	pipe
UW4080	Gungywamp	CT	wall	rock	
UW4081	Gungywamp	CT	chamber	sediment	pipe
UW4083	Hunt's Brook Souterrain	CT	chamber	sediment	pipe
UW4084	Hunt's Brook Souterrain	CT	tunnel	rock	
UW4087	Manitou Hassannash	RI	wall	sediment	pipe
UW4088	Manitou Hassannash	RI	wall	sediment	trowel
UW4089	Manitou Hassannash	RI	cairn	sediment	trowel
UW4091	Ed Wood Estate	RI	cairn	rock	
UW4092	Lewis Hollow	NY	cairn	sediment	trowel
UW4095	Slatersville Rocky Hill Rd	RI	wall	sediment	trowel
UW4098	America's Stonehenge	NH	chamber	sediment	pipe
UW4099	America's Stonehenge	NH	chamber	rock	
UW4100	America's Stonehenge	NH	tunnel	rock	
UW4101	America's Stonehenge	NH	wall	sediment	trowel
UW4102	Crown Farm	RI	wall	sediment	trowel
UW4106	Milford	NH	foundation	rock	
UW4109	Deerfield	NH	Rock pile surrounded by wall	rock	

the sample, but this proved difficult because buried rocks were encountered. Subsequently, samples were collected by trowel and shielded from light by an opaque tarp. For one sample (UW4087-UW4088), both methods were used adjacent to each other.

Rock samples were collected directly from a portion of the structure under an opaque tarp. The rocks had at least one unexposed surface. Presumably the rocks were exposed to light during construction so dating a surface not exposed at present within the structure should date the construction. UW4080, UW4084, UW4099 and UW4100 were taken from a wall of a structure. The outer portion of the rock has been exposed but the inner parts had not been exposed since the structure was built. UW4091 was collected from inside a cairn after several rocks were removed. None of its surfaces had been exposed since construction.

UW4106 was collected from the foundation of a house known to have been constructed between 1740 and 1760. This is the only sample with independent dating information. UW4109 is from an elongated structure with large rocks forming an outside wall and the inside filled with smaller rocks to form a mostly flat platform. Its age is unknown but it is in an area densely settled by Europeans in the late 1700s. It is located about 50 km from UW4106 and could well be about the same age.

3. Methods

The luminescence signal of minerals, such as quartz and feldspar, is a function of natural radioactivity absorbed during burial time. The intensity of the signal is proportional to the age. The amount of radiation necessary to produce the natural luminescence signal (called the palaeodose) is estimated using calibrating laboratory irradiation to obtain an equivalent dose (D_e). Dividing the D_e by the dose rate gives the time the signal was last set to zero, usually by heat or exposure to sunlight. The dose rate (Gy per unit time) is the rate at which the sample absorbs irradiation in its natural setting. It is location specific.

3.1. Dose rate

Natural radiation is composed of alpha, beta, gamma, and to some extent, cosmic radiation.

For coarse-grained material (>~90 μm) in high radiation environments, such as the case here, the bulk of the dose rate comes from beta and gamma radiation. Betas are relatively short-ranged and for rock or sediment samples stem mainly from the sample itself, but gammas have a range of about 30 cm. In complicated geometries such as these rock structures, nearby sediments and rocks as well as the sample contribute to the gamma dose rate. These may vary considerably in their radioactivity. For example, in one cairn that was measured, rocks varied in their potassium (K) content (^{40}K is a principal source of natural radioactivity) from 1.5 to 7%.

Two approaches for estimating the gamma dose rate were applied. One was to collect samples of sediment and rock within about 20 cm of the sample, measure their radioactivity in the laboratory, and use the geometry to reconstruct the dose rate (following Aitken 1985, appendix H, using a density of 1.5 for the sediment and 2.6 for the rocks). The other was to place a $CaSO_4$:Dy dosimeter at the approximate location of the sample and leave it there for one year to directly measure the radioactivity. A drawback of the laboratory method, besides the complicated geometry, is that one cannot see and thus sample what is behind the sample. A drawback of the dosimetry method is that it is difficult to place the dosimeter exactly where the sample was. It was placed in the hole from which the sample was drawn but only at one point while the sample was taken over an area. The radioactivity can vary in this environment over short distances. For example, the calculated dose rates for UW4087 and UW4088, only 10 cm apart, varied from 3.6 to 4.3 Gy/ka. Most confidence was placed in those samples where the two approaches produced statistically identical dose rates.

For the dated rocks, some of the beta dose also comes from outside the sample. There was another rock directly adjacent to the surface being dated for all samples. At the interface between the two rocks, the beta dose rate will be 50% of the beta dose rate from the top rock and 50% of the beta dose rate from the bottom rock. With depth into the rock, the contribution to the beta dose rate of the dated rock increases until after a couple of millimeters, beyond the range of betas that could come from the other rock, all of it does. For UW4091 – one of only three rocks where we could actually obtain a date – such variations in the contribution of the dated and adjacent rock made a difference in the beta dose rate of less than 1%. For UW4106 and UW4109 (the other two for which a date was obtained) no adjacent rock was collected, so it was assumed its beta rate was the same as the collected rock. They were of the same lithology.

For the dated rocks, dosimeters were only placed for UW4084, UW4099, UW4106, and UW4109. It was impossible to collect adjacent rocks for laboratory measurements for these samples without damaging the structure. No dosimeter was placed for the other rock samples (UW4080, UW4091, and UW4100), because there was no practical way to retrieve them (e.g., deep in a cairn). The grain sizes of the rocks were not measured precisely, only roughly by inspecting some of the slices under a low-powered microscope. From this it was estimated the grain size averaged 150–250 μm. This was used to calculate alpha and beta attenuations and the contribution of internal K to the dose rate.

Because single grains were dated for the sediments, another consideration for the beta dose rate is heterogeneity in the distribution of beta emitters. Some grains will receive a higher dose rate than others because they are closer to an emitter or contain an emitter. For K-feldspars, much of this variation probably arises from variation in the percentage of internal K (^{40}K is a significant beta emitter), which can vary from a few to 14% in individual K-feldspar grains. Internal K was not measured on these samples but following Smedley et al. (2012) we assumed an average internal K content of 10%, with an increased one-sigma error of 3% to cover the natural variability in K-feldspar grains. The same was done for the rocks that were dated. For quartz, a

likely source of beta heterogeneity comes from the presence in the sample of K-feldspar grains. If K-feldspar is abundant in unconsolidated sediments and assumed to have a fairly homogenous distribution, the beta irradiation from ^{40}K to quartz is likely to be uniform, but if K-feldspar is not abundant, even if distributed homogenously, some quartz grains will be closer to the ^{40}K emitters than others. The effect of K "hotspot" distribution was modeled after Mayya et al. (2006) and Chauhan et al. (2021), taking into account the beta dose rate and the percentage of betas stemming from K to see how much over-dispersion in a given D_e distribution could be potentially explained by beta heterogeneity. This could have some bearing on the minimum age model used to determine D_e.

Laboratory dose rate measurements used alpha counting, beta counting and flame photometry.

Moisture contents were estimated from measured current values, which varied from 1 to 9%. The samples were relatively dry, being situated under rocks or in structures, but they were collected in late summer so for samples with very low measured content at least 3% moisture was assumed to account for annual variation.

3.2. Equivalent dose

For the sediments, luminescence was measured on 180–212 μm single grains of K-feldspar and quartz. These were prepared following standard procedures in the laboratory under a controlled red- orange light condition. The preparation steps include wet and dry sieving, treatment with HCl and H_2O_2, and density separation using heavy liquids of 2.58 and 2.66 specific gravity for K-feldspars and quartz, respectively. Quartz was additionally etched for 40 min in 48% HF. Given the low sensitivity of quartz (using UV filters) that has been noted in nearby Quebec (e.g.. Lamarche et al., 2007, M. Lamothe, personal communication), we initially thought that only K-feldspars would be useable. However, quartz had a measurable signal in the UV for all samples. Therefore measurements were made using infrared stimulated luminescence (IRSL) for feldspars and optically stimulated luminescence (OSL) for quartz, all on a Risø TL/OSL-DA-20 reader. Stimulation of the K-feldspars was by a 150 mW 830 nm IR laser, set at 30% power and passed through a RG780 filter. Stimulation of quartz was by a 540 nm green laser (45W/cm^2) at 90% power. Stimulations were for 1s. Emission for K-feldspars was measured through a blue filter pack (350–450 nm) and for quartz through a UV340 (ultraviolet) filter. Measurements were made at 125 °C for quartz and 50 °C for feldspar. Signals for both K-feldspar and quartz were collected for 0.8 s, with the first 0.06 s used as the main signal and the last 0.15 s for background.

D_e values were determined using the single-aliquot regenerative (SAR) protocol (Murray and Wintle 2000; Auclair et al., 2003). Regeneration doses ranged from 1 to 20 Gy and a test dose of 3 Gy was employed. Laboratory doses were provided by a ^{90}Sr beta source, calibrated at each single-grain position using quartz gamma-irradiated at Pacific Northwest National Laboratory, Hanford, WA. For quartz, a preheat of 240 °C for 10s was employed after regeneration doses and a 200 °C cut-heat after test doses. For K-feldspars a preheat of 250 °C for 60 s was employed after both regeneration and test doses. After every cycle, the IRSL protocol included a high temperature (325 °C) stimulation using IR diodes for 40s to reduce signal carry over. Dose vs luminescence curves were fit to single saturating exponentials. The SAR protocol was applied to each grain measured, but grains had to meet certain criteria before they were accepted for analysis. The rejection criteria are defined in Tables S1 and S2 in the supplementary material. Reasons for rejection included signals indistinguishable from background, natural signals that did not intersect the dose response curve, failure to reproduce a sensitivity correction from identical doses from the beginning and end of the protocol, significant signal after a zero dose, D_e values that were negative and some positive ones that were indistinguishable from zero (see later discussion), and, for quartz, grains that were identified as feldspars. A dose recovery test was done for both K-feldspar and quartz. This will be discussed in the next section.

K-feldspar suffers from signal loss at ambient temperature called anomalous fading. For older samples, a high temperature IR stimulation, in a method called post-IR-IR (pIRIR), is commonly used to circumvent fading, but the pIRIR signal is known to be difficult to bleach (Buylaert et al., 2012). Because these samples are young and we wanted to ensure some grains were fully bleached, we did not use the pIRIR protocol. Instead, the IRSL signal was measured at low temperature (50 °C) and corrected for fading using the Huntley and Lamothe (2001) method, which is applicable only to younger samples where the dose response curve is in the linear region. We have obtained corrected IRSL ages using 50 °C stimulation that agree with radiocarbon dates for early Holocene sediments (Reuther et al., 2016) and in agreement with OSL dates on quartz for later Holocene sediments (Feathers et al., 2020b), while others have found agreement with independent evidence of corrected IRSL ages as old as 100,000 years (Balescu et al., 2015). Some limited pIRIR data were collected on three samples, using elevated temperatures of 180 and 250 °C. Results are presented in the supplemental material (Table S3). Minimum ages for standard IRSL and the elevated IRSL at 180 °C were in agreement at one-sigma for two samples and at two-sigma for the third, while in two of three cases the minimum age for the elevated IRSL at 250° was significantly older, suggesting an unbleached residual.

Fading was measured on every grain following procedures by Auclair et al. (2003), using regeneration doses of about 30 Gy, test doses of about 10 Gy, and storage times up to 3 days or longer. Ages were corrected for fading on each grain prior to application of any age models.

Because only some of the grains in the samples have been well-bleached before burial, we utilized the minimum age model (Galbraith and Roberts 2012) to determine the D_e of the youngest grains. The central age model (Galbraith and Roberts 2012) was also employed to evaluate central tendency and over-dispersion. Radial graphs of the age distributions among grains were constructed for every sample.

The dated rocks were coarse-grained granitic gneiss (UW4080, UW4084, UW4099, UW4100), granodiorite (UW4091), or granite (UW4106, UW4109). Fig. S3 shows example photos of the rocks. At least three 1.5 cm cores were collected for each sample, under controlled red-orange light conditions, from unexposed surfaces using a diamond tipped 0.5-inch- (~11 mm) diameter drill bit mounted on a drill press. If part of the surface was currently exposed to sunlight, as in some chambers, only unexposed surfaces were sampled. Other rocks, from cairns had no currently exposed surfaces, but the surface sampled was limited to one for which an adjacent rock was collected for dose rate considerations. Granitic gneiss is foliated with alternating layers of lighter and darker minerals. While it might be ideal to collect cores parallel to the foliations, the limitations of what surface could be sampled meant that the cores crosscut the foliations. The cores were cut into ~1 mm slices using a Pace Technology precision saw with a 400 μm thick diamond studded blade. Because some of the rocks were friable, the cores were first impregnated in epoxy before cutting. Small portions (roughly a quarter) were broken off the slices and placed in stainless steel cups to be measured for luminescence on a Risø TL/OSL-DA-15 reader. Not using the whole slice for each measurement allowed repeat measurements on the same slice. D_e was determined by the double SAR method (Banerjee et al., 2001), where an infrared stimulation proceeded a blue stimulation, both using diodes and for 100 s at each step. Emission was through a UV340 filter, and the preheat and test dose were the same as those used for quartz described earlier. A fading test was performed on all slices to correct the feldspar ages. On some samples (UW4080, UW4084 and UW4091) D_e was additionally determined using stimulation just from IR diodes with emission through blue filters (Auclair et al., 2003).

4. Results

4.1. Dose rate

Table S4 gives the relevant concentrations provided by alpha counting and flame photometry. Table S5 compiles information on the beta dose rate determined using two methods and the gamma (plus cosmic) dose rates determined using laboratory and field measurement. It also lists the total dose rate for quartz and k-feldspar. The beta dose rate was (1) calculated from flame photometry and alpha counting assuming secular equilibrium and (2) measured directly by beta counting. The values differed at one-sigma for only four samples (marked in italics in S2), most seriously for UW4092. Because beta counting is a direct measure of beta dose rate, the dose rate was adjusted for these samples by altering the K content to agree with the beta counting. The K-content was altered rather than the U or Th content, because for most samples the beta dose rate was dominated by ^{40}K

Table S5 also compares the gamma and cosmic dose rate determined in two ways. The dosimeters that were placed in the field measure both the gamma and cosmic dose rate. These are compared with the laboratory measured gamma dose rate plus the calculated cosmic dose rate (from Prescott and Hutton 1994). The field measurements are systematically higher for all samples but one. This was also observed on two samples, measured during the same measurement run, from southwestern Washington state, where the deposits are homogeneous. We do not have a reason for this bias, but the dosimeters may be overestimating the dose rate. The effect of the dosimeter measurements on the final dose rates was judged for the sediments by comparing K-feldspar dose rates using only laboratory measurements (plus calculated cosmic) with those using the field dosimeter results for gamma and cosmic dose rates (Table S5 and Fig. 1). Both sets of dose rates share the same laboratory-determined alpha and beta dose rates and the same estimation for percentage of internal K. Both sets of dose rates agreed at one-sigma for six samples, at two-sigma for three samples (although agreement is facilitated by high errors on some samples) and are inconsistent for two samples (UW4089 and UW4102). The data for UW4102 are not plotted in Fig. 1 because the dosimeter reading for this sample was abnormally high, twice that of the next highest reading. The issue of field versus laboratory measurements will be considered further when calculating ages.

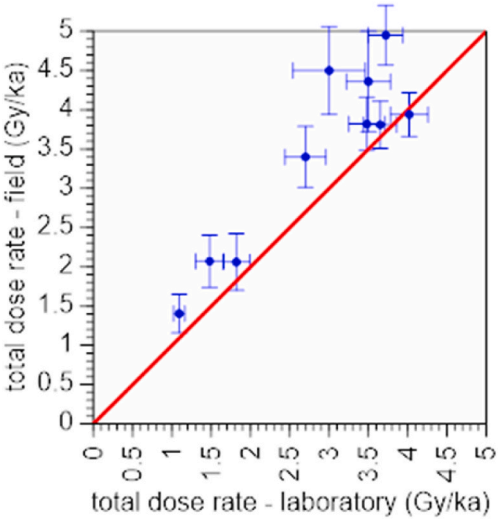

Fig. 1. Comparison of total dose rates between laboratory and field measurements for 10 samples. The red line is 1:1 correspondence. The field dose rate includes laboratory-determined alpha and beta rates.

4.2. Equivalent dose and age – K-feldspars

Fig. S4 gives examples of decay curves from both bright and dim grains and their respective growth curves. The figure also shows examples of fading decay curves.

Table 2 gives the number of accepted grains, the D_e value from the central age model, over-dispersion and the average fading rate for each sample. The samples were relatively sensitive: on average 33% of all grains passed the rejection criteria and were accepted for analysis (Table S1). Most of the rejections were due to poor signal intensities (as defined in the caption to Table S1).

About 2 percent of all the grains were rejected because their D_e was not significantly different from zero. While these may have some bearing on the age of these young samples, most of them were poor precision grains that would not affect over-all statistics. Better precision grains close to but not significantly different from zero were generally accepted. To gauge the effect of rejecting these grains, UW4087, which had more of these rejections percentage-wise than any other sample (11 rejected to 126 accepted), was re-analyzed accepting five of these grains (not including six with negative D_e values, which could not be corrected for fading). The resulting difference in the age from the minimum age model was 10 years.

The over-dispersion, which is a statistical measure of the spread in values, was very high, more than 100% for most samples. While some of this may reflect differential fading rates, the most likely explanation is a wide dispersion in ages (see later discussion).

Average fading rates vary widely among samples. High errors on fading rates are characteristic of single-grains, but other work by this lab on samples from Peru, Alaska, the Aegean, Oman and eastern Washington state (Feathers et al., 2019) has shown that fading rates on individual grains are broadly reproducible. Summary statistics such as those provided by the various age models are particularly reproducible. This was tested on two samples in this study, UW4076 (300 grains) and UW4089 (400 grains). After the standard SAR to determine D_e, a fading test was conducted as done for all samples in this study. Then a second fading test on the same grains was conducted. The ratio of the corrected results from the first and the second estimated g-values for three parameters (central age, over-dispersion, and minimum age) are given in Table S6. The ratio for over-dispersion is not significantly different from one (at one-sigma) for either sample. The ratio for central and minimum ages are not significantly different from one at one sigma for UW4076, and just barely significant at one sigma (but not at two sigma) for UW4089.

Table 3 gives the ages from the central age model and the minimum age model, plus the over-dispersion. Fading was corrected on each individual grain using the Huntley and Lamothe (2001) method. The ages were calculated for most samples using the laboratory derived dose rates, but for samples where using the dose rate from the field dosimetry made a significant difference (more than 1-sigma) in the minimum age,

Table 2
D_e and other data for K-feldspars from the sediment samples.

Sample	# accepted grains	D_e (Gy) (central age model)	Over-dispersion (%)	Fading rate, g_{2days} value, (%/decade) Weighted average
UW4076	316	1.84 ± 0.11	102.2	3.62 ± 11.2
UW4077	183	2.90 ± 0.29	124.1	2.99 ± 0.53
UW4081	250	7.18 ± 0.55	118.2	4.09 ± 0.40
UW4083	182	10.5 ± 0.90	111.3	5.59 ± 0.58
UW4087	126	2.44 ± 0.31	127.2	8.69 ± 0.96
UW4088	217	3.13 ± 0.28	119.0	6.04 ± 0.52
UW4089	177	3.86 ± 0.28	86.4	6.19 ± 0.48
UW4092	155	2.86 ± 0.32	133.2	8.61 ± 0.66
UW4095	166	3.72 ± 0.38	121.4	3.45 ± 0.60
UW4098	234	4.92 ± 0.38	110.5	2.92 ± 2.78
UW4101	106	6.46 ± 0.70	103.1	1.64 ± 5.45
UW4102	246	3.36 ± 0.24	110.2	5.72 ± 0.43

Table 3
Age data for K-feldspars from the sediment samples.

Sample	Age (ka) Central age model	Over-dispersion %	Age (ka) minimum age model	Calendar date (years AD)
UW4076	1.53 ± 0.11	96.7	0.65 ± 0.10	1370 ± 100
With dosimeter	1.08 ± 0.08	95.6	0.51 ± 0.07	1510 ± 70
UW4077	1.89 ± 0.21	120.3	0.40 ± 0.06	1620 ± 60
UW4081	2.74 ± 0.23	113.4	0.53 ± 0.07	1490 ± 70
UW4083	3.36 ± 0.37	108.4	0.60 ± 0.11	1420 ± 110
UW4087	0.90 ± 0.14	96.3	0.60 ± 0.12	1420 ± 120
UW4088	0.84 ± 0.09	104.2	0.23 ± 0.05	1790 ± 50
UW4089	1.44 ± 0.13	76.2	0.59 ± 0.11	1430 ± 110
With dosimeter	1.08 ± 0.10	76.6	0.44 ± 0.08	1580 ± 80
UW4092	1.76 ± 0.26	128.8	0.69 ± 0.08	1330 ± 80
With dosimeter	1.14 ± 0.16	126	0.47 ± 0.05	1550 ± 50
UW4095	1.12 ± 0.12	111.4	0.40 ± 0.04	1620 ± 40
UW4098	2.17 ± 0.20	113.6	0.47 ± 0.10	1550 ± 100
With dosimeter	1.70 ± 0.16	112.0	0.38 ± 0.08	1640 ± 80
UW4101	2.28 ± 0.27	99.8	0.62 ± 0.12	1400 ± 120
UW4102	1.63 ± 0.14	108.1	0.52 ± 0.09	1500 ± 90
With dosimeter	0.60 ± 0.09	112.8	0.19 ± 0.03	1830 ± 30

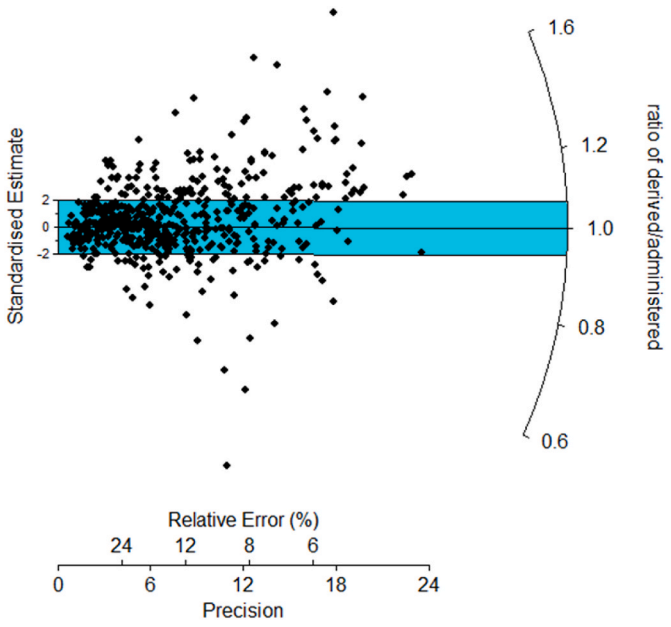

Fig. 2. Radial graph of derived/administered dose in the dose recovery test for K-feldspar single grains. Radial graphs are described in the supplemental material (Fig. S5).

the ages from the latter are also given. There were only four of these. The distributions are displayed as radial graphs in Fig. S5.

The over-dispersion values for the ages are similar to those for equivalent dose. This suggests the high over-dispersion is not the result of differential fading rates. It is more likely a function of differential age, justifying the use of the minimum age model to determine the age of rock placement. The minimum age model requires the input of an over-dispersion value considered characteristic of a single-aged sample. A dose recovery test, where all grains are given an identical dose, was performed to make an estimate of this value, as well as to test the efficacy of the SAR protocol used for these samples. In this test, grains were exposed to first 200s of infrared light from IR diodes (875 nm, 135 mW/cm^2) at 50 °C and then 1s of infrared light from the laser (830 nm 150 mW at 30% power). This seemed to reduce the signal to near background. Then about 5 Gy of beta radiation was applied. The resulting signal was treated as the natural in a subsequent SAR protocol. Comparison of the derived dose with the administered dose serves as a test of the protocol's ability to produce a known dose. The test was applied to eight samples, from which 542 grains passed the acceptance criteria. The results are displayed in terms of the ratio between the derived and administered dose as a radial graph in Fig. 2. The central tendency from the central age model is 1.06 ± 0.02, which represents just a slight overestimation of the administered dose. The scatter was high, however, with an over-dispersion of 30%. This value was used as input for the minimum age model. It is noted that a 15% over-dispersion was also employed, and while this resulted in younger ages than those using 30% over-dispersion, the difference was not significant at one-sigma for any sample. The minimum age model can be run with three or four unknown parameters. Both alternatives were attempted but using four unknowns either produced the same value as using three unknowns or resulted in poor fits for most samples. Where possible the four-parameter alternative was preferred.

The ages from the minimum age model are similar in value for the various samples. Looking at the ages from the minimum age model derived from dose rates just using the laboratory measurements (except cosmic, which is calculated) (Fig. 3, left), all ages but three are consistent with a single age. All but two are consistent with a single age when we substitute the field measurements for gamma and cosmic dose rate for those sample where the lab and field measurements differed significantly (Fig. 3, right), and the distribution looks tighter. One of the outliers in the graph using the field measurements is UW4102, where the reading from the field dosimeter was much higher than the others, as noted earlier. If we assume the field reading is inaccurate, the age for that sample lines up with all the others (see Table 3). The other outlier is UW4088, which was also an outlier when just using the lab measurements for dose rate. That sample was collected only 10 cm from UW4087, where the age was consistent with the others. UW4087 was collected with a tube while UW4088 was collected with a trowel. Perhaps during collection younger grains were introduced into UW4088.

The agreement in derived ages was not expected. It can be explained if the structures were all built within a short period of time. If that is true, then the field measurements of the dose rate must be in general more accurate than the lab measurements since they produced a tighter age distribution. In fact it would be hard to explain why using the field measurements for those sample where these differed from the lab measurements would produce a tighter distribution, if the true ages were not about the same. Construction at the same time seems a more parsimonious explanation than assuming the fading corrections and dose rates are inaccurate and the ages are similar just by coincidence.

If one accepts that the structures were built around the same time, then an estimate of that time can be made by pooling the ages. Leaving out UW4088 and using the lab dose rate measurements for UW4102, the weighted average of the ages displayed in the right graph of Fig. 3 is 0.46 ± 0.03 ka, or AD 1560 ± 30, with no over-dispersion. This is 60 years before the first European settlers arrived. Construction at the same time begs the question why. This will be discussed later but it does imply that these constructions were in response to some common event or series of events.

The shape of the radial graphs can inform on the likelihood that the minimum age model isolates well bleached grains. There are two general patterns in the graphs. One, represented by UW4092 in Fig. 4, is a somewhat bimodal distribution, showing a large number of grains consistent with the minimum age model and a smattering of older grains. Seven of the samples have this kind of distribution. The other pattern, represented by UW4081 in Fig. 4, does not show much of a clump at the young end but rather a more or less even distribution throughout the age range. Five samples show this pattern. The clumping at the young end of the bimodal distributions suggests that these grains represent the youngest possible grains. There are no points below the

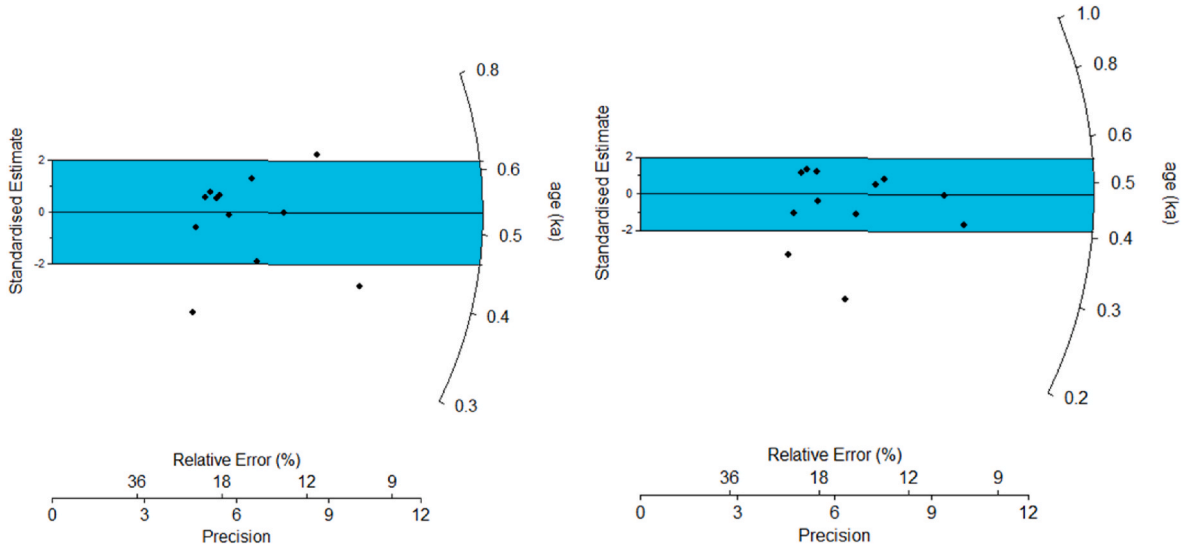

Fig. 3. Radial graphs showing minimum age values for all sediment samples. The ages are derived just using laboratory measurements (and calculated for cosmic) for the dose rate in the left graph. In the right graphs ages are altered for those samples where the lab and field measurements of the gamma and cosmic dose rates differed, using the field measurements. Graphs are at the same scale.

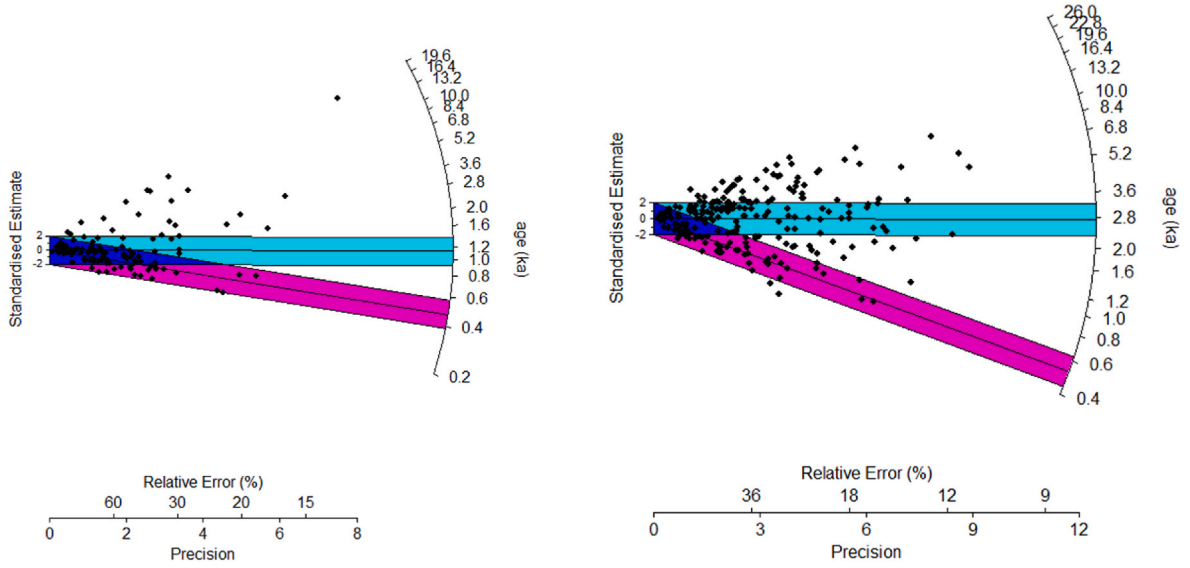

Fig. 4. Radial graphs for the age distribution of K-feldspar grains in UW4092 (left) and UW4081 (right). UW4092 shows a bimodal distribution, while UW4081 shows a more continuous distribution. Pink shading represents points within two standard errors of the age from the minimum age model. Blue shading represents points within two standard errors of the age from the central age model.

line marking the youngest values in the minimum age distribution in the graph, although several points are right at the line or near it. We argue this lower line represents a true limit (within error) of the ages and the minimum age model represents well-bleached grains. Such a limit is less clear for UW4081, where there are two younger grains detected below and only a few at this limit.

However, because there is no difference in minimum ages between the two patterns, it is likely the youngest grains in all samples are well bleached. The older grains in the distributions seem to give Late Pleistocene ages, which is probably the age of the landform the structures sit on.

4.3. Equivalent dose and age – quartz

Fig. S4 show samples of OSL decay curves and their respective growth curves for bright and dim grains.

Table 4 gives the number of grains accepted, the D_e from the central age model, the over-dispersion, and the D_e from the minimum age model for the quartz samples. Quartz was much less sensitive than the K-feldspar, as is typical. Only 9.7% of grains passed the acceptance criteria (compared to 35% for K- feldspar) and it took a lot of machine time to get a statistically large enough sample. A vast majority of the rejects were for poor signal (see Table S2 for details).

A dose recovery test was done on seven samples. The samples were bleached by exposure to the green laser for 1 s. The administered dose was about 5 Gy. A total of 88 grains passed the acceptance criteria (see Table S2). The ratio of derived to administered dose was 1.04 ± 0.3, which is satisfactory, with 9% over-dispersion. The over-dispersion value was much less than was the case for feldspar. Because of micro-dosimetry, this value is probably under-estimated in terms of what might characterize a single-aged sample for applying the minimum age model, but it still seems it should be less than the 30% used for the

Table 4
D_e and other data for quartz from sediment samples.

Sample	# accepted grains	D_e (Gy) central age model	Over-dispersion (%)	D_e(Gy) minimum age model
UW4076	66	2.40 ± 0.24	68.2	0.98 ± 0.16
UW4077	89	1.53 ± 0.20	116.1	0.44 ± 0.07
UW4081	78	5.25 ± 0.76	120.1	0.8 ± 0.08
UW4083	49	4.40 ± 0.81	116.4	1.20 ± 0.34[a]
UW4087	108	1.46 ± 0.18	114.9	0.64 ± 0.04
UW4088	43	0.88 ± 0.13	86.0	0.61 ± 0.05
UW4089	68	4.07 ± 0.52	96.7	0.75 ± 0.08
UW4092	100	1.54 ± 0.18	103.7	0.53 ± 0.09
UW4095	91	2.08 ± 0.26	109.6	0.90 ± 0.05
UW4098	72	2.35 ± 0.35	113.9	0.79 ± 0.15
UW4101	156	3.23 ± 0.25	89.6	0.89 ± 0.09
UW4102	63	2.09 ± 0.32	117.2	0.47 ± 0.10

[a] One outlying point removed.

feldspars. This will be re-evaluated later, but for now Table 4 gives the equivalent dose from the minimum age model using 15% over-dispersion. Radial graphs are shown in Fig. S5. Most samples have the bimodal pattern that was observed for the some of the k-feldspars. Ages are given in Table 5. The ages are computed using the laboratory dose rate data, except for the minimum age for UW4076, UW4089 and UW4092 and UW4098 where the field dosimetry data were used, as justified in the discussion on K- feldspars.

The quartz ages from the minimum age model are systematically younger than the K-feldspar ages, except for UW4076 (Fig. 5). Many are colonial in age, but others are post-colonial, dating to the 19th century. Moreover, unlike the K-feldspar dates, the quartz dates from the various sites are not statistically consistent with a single date. The reasons for the differences between the feldspar and quartz ages will be taken up later.

4.4. Equivalent dose and age – rocks

Of the seven rocks measured, three of them, UW4080, UW4099 and UW4100, yielded very high D_e values at the surface of the rock. This indicates the rocks were either not well-bleached at the time of their placement, or that the bleached surface has eroded since placement (perhaps from freeze-thaw mechanical stress). These three were all granitic gneiss where the cores crosscut the foliations to some degree (Fig. S3). This may also have some bearing on light penetration. Only data from the other four rocks, UW4084, UW4091, UW4106 and UW4109 are presented. The double SAR method provides a D_e value for both IRSL and OSL. Only on one core from UW4091 was an OSL date obtained. On the others either the OSL signal did not pass the acceptance criteria (Table S2) or the OSL signal at the surface was so high as to produce a much older date than from IRSL. The focus here then is on the IRSL signal. Table S7 gives the IRSL D_e and Ln/Tn (signal ratio between the natural and first test dose) as a function of depth for two cores from UW4084 and UW4091, one core from UW4106, and three from UW4109 and the OSL D_e and Ln/Tn for one core from UW4091. Ln/Tn is plotted as a function of depth in Fig. 6 for one core each from UW4084 and UW4091. The points are fit using a luminescence exposure aging model (Sohbati et al., 2012) as explained in the caption. The purpose of the figure is to evaluate the extent of bleaching before burial.

Table 5
Quartz ages from sediment samples.

Sample	Age (ka) central age model	Age (ka) minimum age model	Calendar age (years AD)
UW4076	2.69 ± 0.33	0.66 ± 0.16	1360 ± 160
UW4077	1.22 ± 0.18	0.35 ± 0.06	1670 ± 60
UW4081	1.88 ± 0.29	0.29 ± 0.03	1730 ± 30
UW4083	1.31 ± 0.25	0.36 ± 0.10	1660 ± 100
UW4087	0.48 ± 0.06	0.21 ± 0.02	1810 ± 20
UW4088	0.24 ± 0.04	0.17 ± 0.02	1850 ± 20
UW4089	1.33 ± 0.18	0.17 ± 0.02	1850 ± 20
UW4092	0.65 ± 0.09	0.14 ± 0.03	1880 ± 30
UW4095	0.71 ± 0.10	0.31 ± 0.03	1720 ± 30
UW4098	0.84 ± 0.15	0.28 ± 0.06	1740 ± 60
UW4101	1.34 ± 0.12	0.37 ± 0.04	1650 ± 40
UW4102	0.89 ± 0.15	0.20 ± 0.04	1820 ± 40

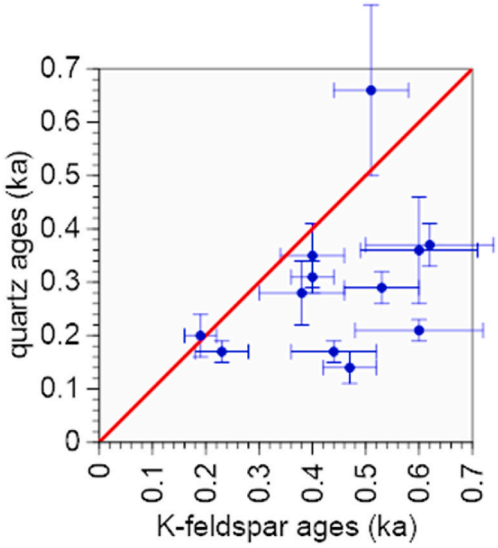

Fig. 5. Comparison of K-feldspar and quartz ages. Red line is 1:1 correspondence.

UW4091 exemplifies a rock that was well bleached at the time it was deposited in the cairn. The Ln/Tn does not change significantly over the first 5 mm depth, indicating that sun exposure was sufficient to empty trapped charge to that depth. Beyond about 7 mm depth, the luminescence signal has not been reduced at all. UW4106 and UW4109 produced similar curves (not shown) except that the extent of bleaching prior to placement was somewhat less (see Table S7). UW4084, on the other hand, only shows a reduced Ln/Tn for the first slice at about 1 mm. While this may represent well-bleaching at the surface, a lack of any plateau does not guarantee it. The one quartz profile, for UW4091, shows a pattern similar to that for feldspar UW4084.

The K-feldspar ages from the rocks had to be corrected for anomalous fading. The fading rate did not change much with depth averaging about 8.7 ± 0.8%/decade for UW4091, 6.7 ± 0.4 for UW4084 and 2.8 ± 0.4. for UW4109. The measured fading rate for UW4106 was about 40%/decade. It was measured twice with the same answer both times. A fading rate this high over the lifetime of this sample is not possible, because a natural signal could not be maintained. A correction would produce an infinite age. The fading rate must have changed through time. For this sample we used the fading rate from nearby rocks to correct the age.

For UW4091, taking a weighted average of the corrected k-feldspar ages from six slices on two cores that were within the well-bleached plateau of the depth curves produced a value of 0.54 ± 0.08 ka, or AD 1490 ± 80, which is a little older but within error terms of the average K-feldspar age from the sediments. The surface slice from the one core from UW4091 that had measurable OSL signal produced an age of 0.39 ± 0.04 ka, or AD 1630 ± 40, in the range of the K-feldspar sediment ages, although like the sediments the quartz age was younger than the feldspar age.

The corrected k-feldspar age from the surface slice of one of the cores for UW4084 is 1.03 ± 0.29 ka, or AD 990 ± 290. This is quite a bit older than the sediment age from the same site, Hunt's Brook Souterrain (UW4083). The sample must have been only partially bleached or the surface eroded.

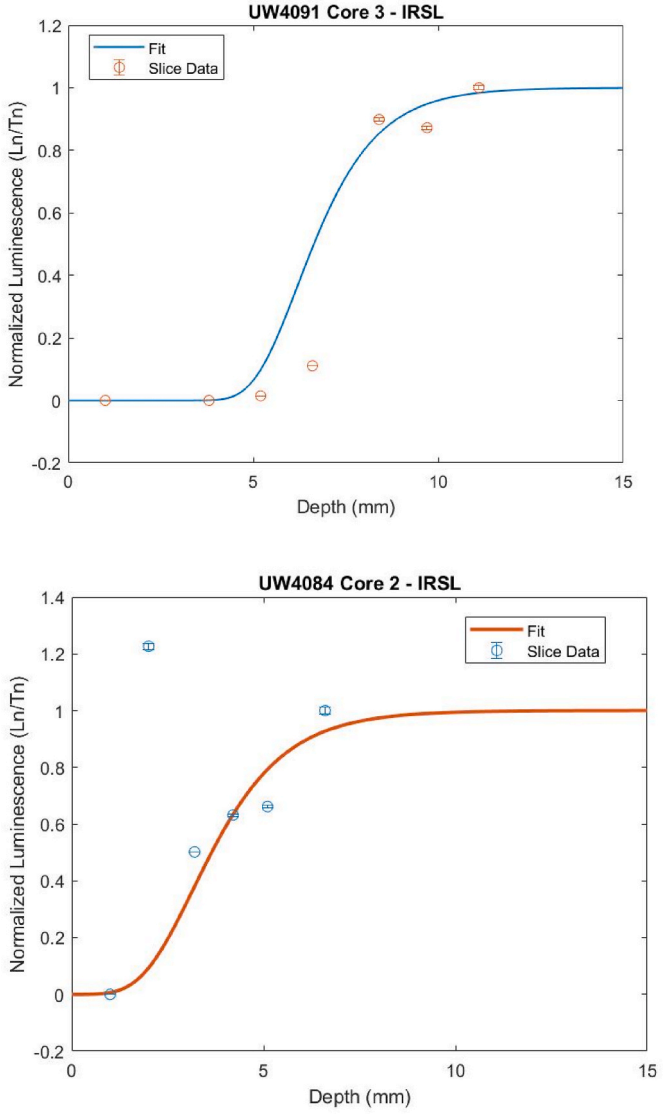

Fig. 6. Depth profiles for rocks from (top) Ed Wood Cairn, RI, (UW4091) and (bottom) Hunt's Brook Souterrain, CT (UW4084). Lines are fits using exposure equation: $L = L_o \exp((-\varphi\sigma_o t)\exp(-\mu x))$, where L_o = saturation level (=1 in this case), $\varphi\sigma$ = product of photon flux and photoionization cross-section, t = time, μ = attenuation coefficient, x = depth. Data is first formatted by measuring the Ln/Tn values for each core slice, then the values are normalized to where the weighted average Ln/Tn values of the deepest two slices equal 1, and the minimum Ln/Tn value equals zero. These data are then fitted to the model using a standard trust-region nonlinear least squares approach, utilizing arbitrary parameter values for the luminescence decay rate constant, time, and the light attenuation coefficient. These fits were not used to determine the age but rather to show the depth of bleaching prior to burial.

Because we had no reliable fading data for UW4106, we first calculated a non-corrected age, using a weighted average of three slices within the well-bleached plateau. This age was 0.24 ± 0.02 ka, or AD 1780 ± 20. We then tried using the fading rate from UW4109 (g = 2.8 ± 0.4), which was the same kind of rock but located 50 km distant. That produced an age of 0.29 ± 0.05 ka, or AD 1730 ± 50. We also tried using the fading rate from another granite rock from another structure located in the same village as UW4106. This sample is not reported here because we could not obtain a date (because of poor bleaching or erosion) but it did yield a fading rate of 4.2 ± 0.3. This gave an age of 0.32 ± 60 ka, or AD 1700 ± 60. All these ages are within error terms of the known construction date of AD 1740-60. It is unfortunate that the one sample with a known age had poor fading data, but it is encouraging that the right age could be obtained using fading rates from nearby rocks. For UW4109, taking the weighted average of five ages from the top two slices of three different cores yielded an age of 0.28 ± 0.02 ka, or AD 1740 ± 20. Although the true age of this structure is unknown, it was thought likely that it is about the same age as UW4106. This appears to be the case.

Using the double SAR method means that the IRSL was measured through an ultraviolet filter. The blue emission is generally preferred for IRSL because the UV emission appears to have higher fading rates (e.g., Devi et al., 2022). Standard IRSL measurements using blue filters were made on three samples. For UW4080, the blue emission was as poorly bleached as the UV emission. For UW4084, the blue emission provided a D_e value of 1.24 Gy and the date of 1.03 ka mentioned earlier, while the UV emission, although on a different core, gave a D_e value of 14 Gy. UW4091 provided a direct comparison as portions of the same core (different from the one depicted in Fig. 6) were measured both ways. Using the UV emission, portions of the first six slices provided an age of 0.55 ± 0.07 ka (weighted average), while different portions of the same slices, using the blue emission, gave an age of 1.34 ± 0.41 ka (although the fading rates were less). The younger date is more similar to other dates reported in this study. Both UW4106 and UW4109 used the UV emission but provided ages agreeing, reasonably, with expectations. Although difficult to judge from these sparse data, nothing seems to indicate that the UV emission cannot provide reliable results.

5. Discussion

Except for rocks from one historic structure and one likely historic structure, the rock samples provided little chronological resolution for the other structures because most were poorly bleached, either because of poor exposure to sunlight at the time of their placement, subsequent erosion or lithological issues. The one rock sample that did appear well-bleached at placement yielded an age that agreed with the K-feldspar ages of the sediments. The sediment feldspars provided similar ages for sites across New England. The quartz ages were younger and more varied. Better understanding of this discrepancy is warranted because resolution is required to show whether the structures are pre-colonial.

Quartz is known to bleach faster than feldspar, so one explanation is that the feldspar signals in these samples are less bleached than the quartz. But the ages were based on the minimum age model, where the best bleached grains are isolated, and arguments were given earlier of why the youngest feldspar grains appeared well bleached.

Because the average fading rate, or g-value, is rather high for some samples (Table 2), a reviewer raised the possibility that the IR ages might be over-estimated, citing some literature that suggests high fading rates lead to over-estimated ages when corrected (Reimann et al., 2011). This might be sample specific because other work does not find such over-estimation (Huntley and Lamothe 2001). To check this for these samples, the central age and minimum age models were re-applied to two samples with high weighted average g-values (6.2–8.6%/decade) but this time removing all grains with g-values greater than 5. A comparison between using all grains and just those with $g < 5$ of the ages from these models and the over-dispersion is shown in Table S8. There are no significant differences. Ignoring the error term, the MAM for UW4092 is younger for <5 g grains than for all grains, but still much older than the quartz age. I conclude that over-estimation of the age because of high fading rates cannot explain the difference between the quartz and feldspar ages.

Heterogeneity in the distribution of beta irradiation is a problem for single-grain dating because of the relatively short range of beta radiation compared to gamma radiation (the effect of alpha radiation is not very significant for coarse-grain samples). A principal cause of heterogeneity for K- feldspars is probably variation in the percentage of internal K of the feldspars themselves, which can be accounted for by increasing the error on the estimation of percent internal K. The k-feldspars can be a

problem for the quartz, however, and their distribution in the sediment can be a main cause of beta heterogeneity for quartz (Mayya et al., 2006)., particularly if they are low in abundance. Beta radiation from the U and Th series, on the other hand, is usually assumed to be more evenly distributed. Mayya et al. (2006) proposed a model, recently updated by Chauhan et al. (2021), to evaluate the effect on dose rate to individual grains in the presence of unevenly distributed K- feldspars. Others (David et al., 2007; Feathers et al., 2020a) have used this model, using the proportion of beta dose rate to total dose rate and the proportion of beta dose rate stemming from K, to test whether the observed distribution of D_e values could be explained by beta heterogeneity. We applied this to seven samples using the finite mixture model (Galbraith and Roberts 2012) to define the structure of the distribution. We used the Mayya et al. model to adjust the dose rate of the lowest component of the finite mixture model (similar to the minimum age) on the assumption these grains were far from K-feldspar hotspots. We then compared the adjusted age to the age of the 2nd component (which is about the same magnitude as the central age). In no cases could the adjusted age come anywhere near to matching the age of the 2nd component, indicating that by this model beta heterogeneity could not explain the differences in D_e of the components. Nevertheless, in case this model underestimates possible heterogeneity, we increased the over-dispersion value typical of a single-age sample in the minimum age model from 15% to 30% (same as used for the feldspars) to gauge the effect on the quartz ages. Such increase did not make a significant difference for any sample except UW4083 (which suffered from small quartz sample size) and UW4102 (which is one sample where the feldspar and quartz ages are close to agreement). Microdosimetry does not seem able to explain the young ages of the quartz for the other samples.

The quartz signal is composed of several components based on their bleachability (Jain et al. 2003). The SAR method for determining D_e in quartz was designed to work on the fast-bleaching component and is strictly applicable only to quartz signals dominated by that component (Wintle and Murray 2006). A commonly referenced model of that kind of signal is the Risø calibration quartz from a Danish beach sand. The shape of the quartz decay curves on single grains for two samples, UW4087 and UW4101, were compared with the Risø quartz standard using linear modulated OSL (LM-OSL). In conventional OSL, the power of the stimulating laser is kept constant during measurement, but in LM-OSL the power is ramped from zero to maximum during measurement. This facilitates visual separation of the components, because the fast component empties much earlier than slower components. Here the laser was ramped from 0 to 90% power in 30s (Fig. 7). In this mode, the Risø standard shows a sharp peak centered at about 1.8 s (5.4% power), dropping to a low value by 5.4 s (16.2% power). Where a slower bleaching component is significant, the drop from the peak value is much less. The ratio of the 5.4 s signal to the 1.8s signal for the Risø standard (n = 98) is on average 0.29 ± 0.13, where it is 0.55 ± 0.43 for UW4087 (n = 28) and 0.39 ± 0.33 for UW4101 (n = 62). Both samples have signals with significant slower components, although there is lots of variation. Fig. 7 shows LM-OSL quartz for the three samples, selecting grains with the average ratio. UW4087 clearly has a different shape than the Risø curve. The curve for UW4101 is similar to that for Risø but has a shoulder on the main peak that probably represents a slower component. This could explain younger quartz grains in the New England samples if younger grains correlate with higher ratios, and if significant contribution of slower components to the signal results in underestimation of the age. However, this is not the case for UW4087 although it is the case for UW4101. For the latter sample, grains with ratios less than 0.4 (more dominance by fast component) have an average D_e of 3.4 ± 0.6 Gy compared to those with ratios greater than 0.4 of 2.7 ± 0.4 Gy. Recent work (Rajapara et al. 2022) has suggested that samples with a significant slower component can underestimate the age because of sensitivity change of the natural signal.

To try to isolate the fast component as much as possible from the other components, the integration limit of the signal for UW4095 was reduced to just one channel at the decay peak, representing 0.017s of initial exposure. Doing, this the minimum age was actually reduced, by 19%, not increased, although the difference was not significant at one-sigma.

Another way to look at this is by using the fast ratio, a ratio of signal measured early on a conventional OSL decay curve and of a signal measured later on (Duller 2012). This was done on two samples, UW4081 and UW4087, plus the Risø standard, using the signals at 0.02 s and 0.22–0.26 s, with the signal at 0.70–1.0 s subtracted as background. The ratio will increase for samples dominated by a fast component. Fig. 8 shows the distribution of fast-ratio values. While mean values do not vary much, the distribution from UW4081 and UW4087 extends to much lower values than it does for the Risø standard. Also, in both UW4081 and UW4087 the ratio tended to increase with D_e, shown for UW4081 (Fig. 9), although with a lot of scatter.

The data suggest that quartz signal decay curves for many grains in the New England samples do not conform to that expected if dominated by the fast component. These data are not as conclusive as they could be because the intensities of the quartz signals are so low. Fig. 10 compares the quartz and feldspar intensities for UW4081 and UW4092. The feldspar signal is 2–3 orders of magnitude larger than the quartz signals. Such low quartz signals make truly young grains difficult to distinguish

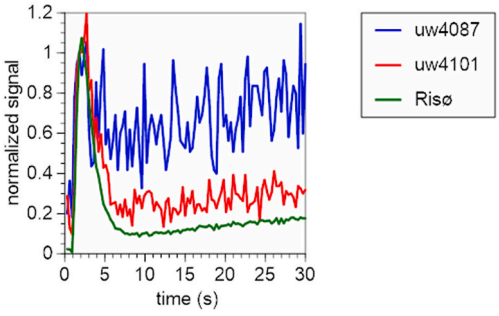

Fig. 7. Normalized linear modulated OSL for three quartz grains, from UW4087, UW4101 and Risø quartz standard. The ratios of the signal at 5.4 and 1.8s is 0.62, 0.40, and 0.20 respectively. Normalization is by the signal at 1.8 s, which is the peak for most grains from the Risø standard but varies from grain to grain. Greater fluctuations in the curves for UW4087 and UW4101 are due to a much lower intensity signal compared to that for the Risø standard.

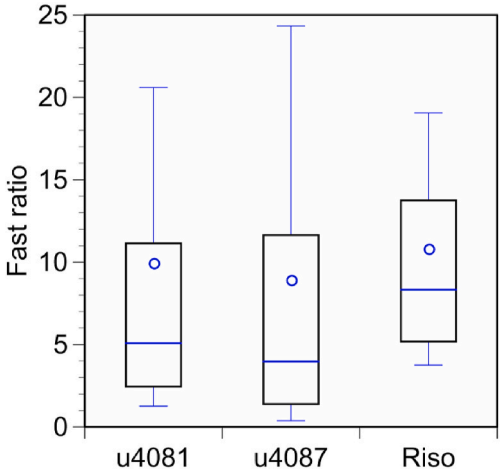

Fig. 8. Box plots showing fast ratio distribution of two samples plus the Risø standard. The box lines from bottom to top represent the 10th 25th, 50th (median), 75th and 90th percentiles, while the open circle represents the mean. Negative values, caused by high backgrounds are excluded. No negative values were obtained for the Risø standards, but 12% of UW4081 values and 24% of UW4087 values were.

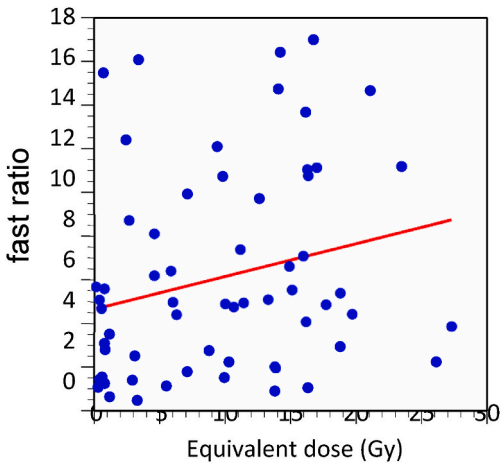

Fig. 9. Fast ratio as a function of D_e (Gy) for UW4081. Fast ratios greater than 18 were excluded for ease of presentation.

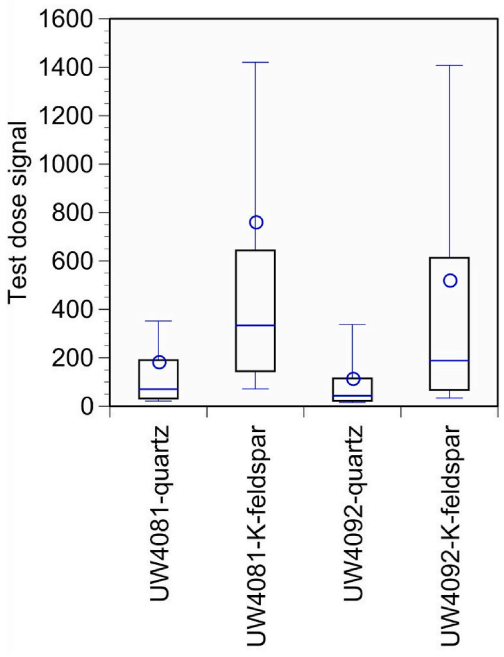

Fig. 10. Box plots showing intensity of quartz versus feldspar for UW4081 and UW4092. The signal (integrated over fhe first 0.06s) from the first test dose (about 3 Gy) was used to compare intensities. The box lines from bottom to top represent the 10th 25th, 50th (median), 75th and 90th percentiles, while the open circle represents the mean.

from those where intensity is just too low for good resolution.

If the discrepancy between the quartz and feldspar signals cannot be fully explained, the quartz signals certainly have issues. The feldspar signals have fewer problems and also provide a consistency in ages that the quartz signals does not provide. While in itself not a reason to reject the quartz dates, to accept the quartz ages, one has to explain why all the feldspar ages are the same. As argued earlier, that the structures are really about the same age is the most parsimonious explanation. If that is true, then the quartz ages cannot be right. Dates on sediments obtained by Mahan et al. (2015,2020) for Upton Chamber and Pratt Hill in Upton, MA, Tolba site near Leverett, MA, and Hopkinton Preserve, RI, range from AD 1450–1650, based on minimum age models. These are in the same range as the feldspar dates of AD1570–1610 reported here. Interestingly, Mahan used mainly quartz, although some feldspar ages agreed with the quartz.

There have been seven radiocarbon dates obtained at America's Stonehenge and three at Gungywamp (published in Bulletin of the Early Sites Research Society, 1991), all on charcoal, but only one of the radiocarbon dates, from America's Stonehenge, agrees with the luminescence dates reported here. Others are earlier or later. Because of problems of associating the charcoal with the construction event, there is no reason to expect any of the radiocarbon ages are correct.

An additional issue raised by a reviewer concerns the assumption that placement of the rock put an end to turbation processes so that the youngest grains represent the placement date. The reviewer thought there could be continual rejuvenation of these sediments with younger grains through lateral migration even if sealed by the rock. In previous work, the senior author tested the extent of lateral movement under rocks on the Great Plains by comparing ages obtained from sediments under the center of the rock to those near the edge of the rocks (Feathers et al., 2015). No significant difference was found. Others have used this assumption to date sediments under rocks as well (e.g., Holzer et al., 2010, Kemp et al., 2022, Outram et al., 2010, Porat et al., 2006, Vafiadou et al., 2007), but these are mostly more arid environments than New England, so perhaps continuous rejuvenation is not a major concern in these studies. We have one way of testing this for the New England samples. The degree of rejuvenation must be partly a function of depth, with shallower sediments more likely to have significant lateral movement of young grains than deeper ones. All but one of the samples in this study varied in depth from 5 to 37 cm with the medium depth 21–24 cm. The rocks are variously embedded into the ground. The exception was UW4083, which was taken from inside a chamber, containing no visible organic matter, and that was 2 m below the current ground surface. If the rejuvenation hypothesis is correct, we should find, all else being equal, younger dates associated with shallower samples. But all the dates are statistically the same. The sample from UW4083 at 2 m depth is the same age (0.60 ka) as the sample from UW4101 at 5 cm depth (0.62 ka). Of course maybe they are not really same age. W4191 is actually much older but more intense rejuvenation has made it appear the same age as UW4083. One could make a similar argument for other uncertainties such as dose rates and fading rates. All these variables would have to conspire to produce values that make it appear these samples are the same age when in reality they are not. Such a remarkable coincidence must be rejected on grounds of parsimony.

While dating these structures does not say who built them, the dates do constrain the possibilities. The AD 1560 ± 20 date rules out colonial settlers. They began settling the coastal regions of Massachusetts in 1620–1630, but reached inland only a couple decades later. There were other European visitors to the Northeast prior to AD 1620, including the Vikings (an archaeological site in Newfoundland dates to AD1000, Nydal, 1989), Basque fishermen, and various English, French and Dutch explorers in the mid to late 1500s and early 1600s. For example, Giovanni da Verrazzano, an Italian in service of France, explored the southern New England coast in 1524 (Morison 1971). Also, Jacques Cartier, a Breton-French explorer made three voyages to what is now Quebec between 1534 and 1541, sailing up the St. Lawrence River as far as present day Montreal, establishing a fort near today's Quebec city, and having several encounters with the native Iroquois (Biggar 1924). Weidensaul (2012) gives a review of interactions between early Europeans and native Americans. The French founded Quebec in 1608, following a short-lived colony on Saint Croix Island in eastern Maine in 1604 (Bishop 1948). But there is no evidence of sustained European settlement in New England prior to 1620. That leaves the ancestors of modern native Americans as the likely builders of the structures.

The feldspar ages suggest that the structures sampled in this study were constructed at about the same time. This implies a common reason for their construction. The use of these structures has been widely speculated about, with varying plausibility, but unchallenged evidence is hard to come by. To add to this speculation, I note that the building of these structures corresponds to the earliest contact with Europeans. There is no question that such contact resulted in disruptions to native

societies, but when that disruption happened is subject to debate. Epidemics from European pathogens was a major disruptor. The first widely recognized epidemic in the Northeast occurred in coastal New England in 1616–1619, causing depopulation before the arrival of the Pilgrims (Snow and Lanphear 1988; Marr and Cathey 2010). If these structures can be construed as sanctuaries or places of refuge from widespread death, this could explain why they might be the same age. This epidemic was confined to the coast and is later than our average date. Early records (Biggar 1924) suggest some deaths among natives and Europeans during the Cartier voyage in 1535. Dobyns (1983) suggests several other epidemics during the 16th century, based on a 1630 document, giving only indirect evidence by Roger Williams, colonizer of Rhode Island. Ramenofsky (1987), reviewing archaeological evidence for population decline among the Iroquois in central New York, concludes that population decline was certainly underway by the early 1600s, but that earlier decline cannot be discounted. Other archaeologists (Jones 2010a, b and Snow and Starna 1989) maintain there was no significant population decline among the Iroquois until the 1600s and in fact there was increase in the 1500s. But the latter could reflect in-migration from other areas suffering population loss. The structures could also be a response to other disruption to traditional culture caused by European contact, for example increased warfare among native groups. Iroquois settlements increasingly included defensive structures after about AD 1500 (Jones 2010a). The formation of the Iroquois confederacy, an amalgamation of previously independent groups is also seen as a response to European contact (Starna, 2008) – possibly also related to disease –but when that happened is contested. At any rate, whether or not these structures are related to European contact is beyond the scope of this paper. We mention it only as an example of how an argument for the structures being the same age could be made.

6. Conclusions

Luminescence dating was applied to sediments and rocks from several rock structures in New England. The sediments were collected from directly underneath rocks in an attempt to date the placement of the rock. The dated rocks were part of the structures themselves.

The radiation environment for these samples was complex, but combination of *in situ* dosimeters and laboratory measurements produced relatively consistent results for most samples.

Luminescence of the sediments was measured on single grains, using both quartz and K- feldspars. D_e was determined by SAR and the age was derived from the minimum age model. Ages were corrected for fading on the feldspars. The feldspar ages from 11 samples were consistent with a single age. The weighted average was AD 1560 ± 20. The quartz ages were systematically younger and covered a wider range of dates including some in the 19th century. The quartz signals were generally weak and many of them did not appear to be dominated by the fast component. These issues cast doubt on the validity of the quartz ages. The feldspars, on the other hand, did not appear to have serious problems.

Of the seven rocks measured, four did not appear to have been well bleached at the time of their placement. Only three rocks appeared to have been well bleached. One produced an age in agreement with the feldspar ages. Of the other two, one was from an historic structure of known 18th century age. Uncertainty in the fading rate prevented a conclusive age but using fading rates from nearby rocks produced ages in agreement with the known age. The other, from a likely historic structure, also produced an 18th century age.

The ages support building of the other structures prior to colonial settlement, probably by native American groups.

Contribution of authors

J. Feathers was responsible for all laboratory measurements and the writing of the paper. M. Frouin helped with sample collection and with the writing. T. Bench did the fitting for the depth profile curves of the rocks and also helped with the writing.

Availability of data

Any data can be obtained from J. Feathers upon request (jimf@uw.edu).

Declaration of competing interest

The authors declare that they have no known competing financial interests or personal relationships that could have appeared to influence the work reported in this paper.

Acknowledgments

This project was funded by the New England Antiquities Research Association (NEARA). Collection of the samples was organized by NEARA members, particularly through the efforts of its president, Harvey Buford. The content of the paper, however, is solely the responsibility of the authors. The analytical work was done at the University of Washington.

Appendix A. Supplementary data

Supplementary data to this article can be found online at https://doi.org/10.1016/j.quageo.2022.101402.

References

Aitken, M.J., 1985. In: Thermoluminescene Dating. Academic Press, Oxford.
Auclair, M., Lamothe, M., Huot, S., 2003. Measurement of anomalous fading for feldspar IRSL using SAR. Radiat. Meas. 37, 487–492.
Balescu, S., Huot, S., Mejri, H., Barre, M., Forget Brisson, L., Lamothe, M., Oueslati, A., 2015. Luminescence dating of Middle Pleistocene (MIS 7) marine shoreline deposits along the eastern coast of Tunisia: a comparison of K-feldspar and Na-feldspar IRSL ages. Quat. Geochronol. 30, 288–293.
Banerjee, D., Murray, A.S., Bøtter-Jensen, L., Lang, A., 2001. Equivalent dose estimation using a single aliquot of polymineral fine grains. Radiat. Meas. 33, 73–93.
Biggar, H.P. (Ed.), 1924. The Voyages of Jacques Cartier, Published from the Originals with Translations, Notes, and Appendices. Publications of the Public Archive of Canada 11, Ottawa.
Bishop, M., 1948. In: Samuel de Champlain: the life of fortitude. Knopf, New York.
Buylaert, J.-P., Jain, M., Murray, A.S., Thomsen, K.J., Thiel, C., Sohbati, R., 2012. A robust feldspar luminescence dating method for Middle and Latge Pleistocene sediments. Boreas 41, 435–451.
Chauhan, N., Selvam, T.P., Anand, S., Shinde, D.P., Mayya, Y.S., Feathers, J.K., Singhvi, A.K., 2021. Distribution of natural beta dose to individual grains in sediments. Proc. Indian Nat. Sci. Acad. https://doi.org/10.1007/s43538-021-00057-y.
David, B., Roberts, R.G., Magee, J., Mialanes, J., Turney, C., Bird, M., White, C., Fifield, L.K., Tibby, J., 2007. Sediment mixing at Nonda Rock: investigations of stratigraphic integrity at an early archaeological site in northern Australia and implications for the human colonisation of the continent. J. Quat. Sci. 22, 449–479.
Devi, M., Chauhan, N., Rajaparu, H., Joshi, S., Singhvi, A.K., 2022. Multispectral athermal fading rate measurements of K-feldspar. Radiat. Meas. 156, 106804.
Dobyns, H., 1983. In: Their Number Become Thinned. The University of Tennessee Press, Knoxville.
Duller, G.A.T., 2012. Improving the accuracy and precision of equivalent doses determined using the optically stimulated luminescence signal from single grains of quartz. Radiat. Meas. 47, 770–777.
Feathers, J.K., Zedeño, M.N., Todd, L., Aaberg, S.A., 2015. Dating stone alignments by luminescence. Adv. Archaeol. Pract. 3, 378–396.
Feathers, J.K., More, G., Solis, P., Burkholder, J.E., 2019. IRSL dating of rocks and sediments from desert geoglyphs in coastal Peru. Quat. Geochronol. 49, 177–183.
Feathers, J.K., Evans, M., Stratford, D.J., de la Peña, P., 2020b. Exploring complexity in luminescence dating of quartz and feldspars at the Middle Stone Age site of Mwulu's Cave (Limpopo, South Africa). Quat. Geochronol. https://doi.org/10.1016/j.quageo.2020.101092.
Feathers, J.K., Biehl, S.M., Kline, S., Lepper, B.T., 2020a. Preliminary report of a luminescence date for a Hopewell ceremonial clay basin from Seip-Pricer Mound. Curr. Res. Ohio Archaeol. 2020.
Feder, K.L., 2019. In: Archaeological Oddities: a Field Guide to Forty Claims of Lost Civilizations, Ancient Visitors, and Other Strange Sites in North America. Rowland and Littlefield, Lanham, MD.

Galbraith, R.F., Roberts, R.G., 2012. Statistical aspects of equivalent dose and error calculation and display in OSL dating: an overview and some recommendations. Quat. Geochronol. 11, 1–27.
Hoffman, C., 2019. In: Stone Prayers: Native American Constructions of the Eastern Seaboard. Arcadia Publishing, West Columbia, SC.
Holzer, Assaf, Avner, Uzi, Porat, Naomi, Horwitz, Liora Kolska, 2010. Desert kites in the negev desert and Northeast sinai: their function, chronology and ecology. J. Arid Environ. 74, 806–817.
Huntley, D.J., Lamothe, M., 2001. Ubiquity of anomalous fading in K-feldspars and the measurement and correction for it in optical dating. Can. J. Earth Sci. 38, 1093–1106.
Ives, T.H., 2013. Remembering stone piles in New England. Northeast Anthropol. 79–80, 37–80.
Ives, T.H., 2015. Cairnfields in New England's forgotten past. Archaeol. E. N. Am. 43, 119–132.
Jain, M., Murray, A.S., Bøtter-Jensen, L., 2003. Characterization of blue-light stimulated luminescence components in different quartz grains: implications for dose measurement. Radiat. Meas. 37, 441–449.
Jones, E.E., 2010a. Population history of the Onondaga and Oneida Iroquois, AD 1500-1700. Am. Antiq. 75, 387–407.
Jones, E.E., 2010b. Sixteenth- and seventeenth- century Haudenosaunee (Iroquois) population trends in northeastern North America. J. Field Archaeol. 35, 5–18.
Kemp, J., Olley, J., Stout, J., Pietsch, T., 2022. Dating sone arrangements using optically stimulated luminescence and fallout radionuclides. Geoarchaeology 37, 1–11.
Lamarche, L., Bondue, V., Lemelin, M.-J., Lamothe, M., Roy, A.G., 2007. Deciphering the Holocene evolution of the St. Lawrence River drainage system using luminescence and radiocarbon dating. Quat. Geochronol. 2, 155–161.
Mahan, S.A., 2020. In: Optically Stimulated Luminescence (OSL) Data and Ages for Selected Native American Stone Landscape Features: Final Project Report Submitted to the Narragansett Indian Tribal Historic Preservation Trust. U. S. Geological Survey, Department of the Interior, USA.
Mahan, S.A., Martin, F., Taylor, C., 2015. Construction ages of the Upton Stone Chamber: preliminary findings and suggestions for future luminescence research. Quat. Geochronol. 30, 422–430.
Marr, J.S., Cathey, J.T., 2010. New hypothesis for cause of epidemic among Native Americans, New England, 1616-1619. Emerg. Infect. Dis. 16, 281–286.
Mayya, Y., Morthekai, P., Murari, M.K., Singhvi, A., 2006. Towards quantifying beta microdosimetric effects in single-grain quartz dose distribution. Radiat. Meas. 41, 1032–1039.
Moore, C.M., Weiss, M.V., 2016. The continuing "stone mound problem": identifying and interpreting the ambiguous rock piles of the Upper Ohio Valley. J. Ohio Archaeol. 4, 39–71.
Morison, S.E., 1971. In: The European Discovery of America: the Northern Voyages. Oxford University Press, New York.
Murray, A.S., Wintle, A.G., 2000. Luminescence dating of quartz using an improved single-aliquot regenerative-dose protocol. Radiat. Meas. 32, 57–73.
Neudorfer, G., 1979. Vermont' stone chambers: their myth and their history. Vt. Hist. 47, 79–147.
Nydal, Reidar, 1989. A critical review of radiocarbon dating of a Norse settlement at L-Anse Aux Meadows, Newfoundland, Canada. Radiocarbon 31, 976–985.
Outram, Zoe, Batt, Catherine M., Rhodes, Edward J., Dockrill, Stephen, 2010. The integration of chronological and archaeological information to date building construction: an example from shetland, scotland, UK. J. Archaeol. Sci. 37, 2821–2830.
Porat, Naomi, Rosen, Steven A., Boaretto, Elisabetta, Avni, Yoav, 2006. Dating the ramat saharonin late neolithic desert cult site. J. Archaeol. Sci. 33, 1341–1355.
Rajapara, H.M., Chauhan, N, Feathers, J, Garnett, S.T., Wasson, R.J., Jaiswal, M.K., Gajjar, P.N., Singhvi, A.K., 2022. How robust are SAR single grain paleo-doses? The role of changes in luminescence sensitivity. Quat. Geochronol. Submitted for publication.
Ramenofsky, A.F., 1987. In: Vectors of Death; the Archaeology of European Contact. University of New Mexico Press, Albuquerque.
Reimann, T., Tsukamoto, S., Naumann, M., Frechen, M., 2011. The potential of using K-rich feldspars for optical dating of young coastal sediments – a test case from Darss-Zingst peninsula (southern Baltic Sea coast. Quat. Geochronol. 6, 207–222.
Reuther, J.D., Potter, B.A., Holmes, C.E., Feathers, J.K., Lanoë, F.B., Kielhofer, J., 2016. The Rosa-Keystone Dunes Field: the geoarchaeology and paleoecology of a late Quaternary stabilized dune field in Eastern Beringia. Holocene 26, 1939–1953.
Smedley, R.K., Duller, G.A.T., Pearce, J.G., Roberts, H.M., 2012. Determining the K-content of single- grains of feldspar for luminescence dating. Radiat. Meas. 47, 790–796.
Snow, D.R., Lanphear, K.M., 1988. European contact and Indian depopulation in the Northeast: the timing of the first epidemics. Ethnohistory 35, 15–33.
Snow, D.R., Starna, W.A., 1989. Sixteenth century depopulation: a view from the Mohawk Valley. Am. Anthropol. 91, 142–148.
Sohbati, R., Murray, A.S., Chapot, M.S., Jain, M., Pederson, J., 2012. Optically stimulated luminescence (OSL) as a chronometer for surface exposure dating. J. Geophys. Res. Solid Earth 117 (B9).
Starna, W.A., 2008. Respecting the origins of the league of Iroquois. Proc. Am. Phil. Soc. 152, 279–321.
Vafiadou, Asimina, Murray, Andrew S., Liritzis, Ionnis, 2007. Optically stimulated luminescence (OSL) dating investigations of rock and underlying soil from three case studies. J. Archaeol. Sci. 34, 1659–1669.
Weidensaul, S., 2012. In: The First Frontier: the Forgotten History of Struggles, Savagery and Endurance in Early America. Houghton, Mifflin, Harcourt, Boston.
Wintle, A.G., Murray, A.G., 2006. A review of quartz optically stimulated luminescence characteristics and their relevance to single-aliquot regeneration dating protocols. Radiat. Meas. 41, 3639, 391.